JACS
JOURNAL OF THE AMERICAN CHEMICAL SOCIETY
Article
pubs.acs.org/JACS

Quantitative Analysis of the Role Played by Poly(vinylpyrrolidone) in Seed-Mediated Growth of Ag Nanocrystals

Xiaohu Xia,[†,‡,§] Jie Zeng,[†,§] L. Kyle Oetjen,[†] Qingge Li,[‡] and Younan Xia*[,†,⊥]

[†]Department of Biomedical Engineering, Washington University, St. Louis, Missouri 63130, United States

[‡]Engineering Research Center of Molecular Diagnostics, School of Life Sciences, Xiamen University, Xiamen, Fujian 361005, P. R. China

Supporting Information

ABSTRACT: This article presents a quantitative analysis of the role played by poly(vinylpyrrolidone) (PVP) in seed-mediated growth of Ag nanocrystals. Starting from Ag nanocubes encased by {100} facets as the seeds, the resultant nanocrystals could take different shapes depending on the concentration of PVP in the solution. If the concentration was above a critical value, the seeds simply grew into larger cubes still enclosed by {100} facets. When the concentration fell below a critical value, the seeds would evolve into cuboctahedrons enclosed by a mix of {100} and {111} facets and eventually octahedrons completely covered by {111} facets. We derived the coverage density of PVP on Ag(100) surface by combining the results from two measurements: (i) cubic seeds were followed to grow at a fixed initial concentration of PVP to find out when {111} facets started to appear on the surface, and (ii) cubic seeds were allowed to grow at reduced initial concentrations of PVP to see at which concentration {111} facets started to appear from the very beginning. We could calculate the coverage density of PVP from the differences in PVP concentration and the total surface area of Ag nanocubes between these two samples. The coverage density was found to be 140 and 30 repeating units per nm^2 for PVP of 55 000 and 10 000 g/mol in molecular weight, respectively, for cubic seeds of 40 nm in edge length. These values dropped slightly to 100 and 20 repeating units per nm^2, respectively, when 100 nm Ag cubes were used as the seeds.

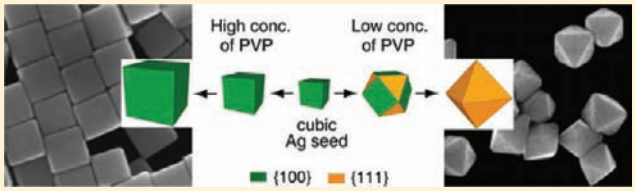

1. INTRODUCTION

Noble-metal nanocrystals with controlled sizes and shapes have received great interest in recent years due to the strong correlations between the size and shape of a nanocrystal and its electronic, optical, magnetic, and catalytic properties.[1−8] The interest has also been augmented by the technological applications of these nanocrystals in various areas including catalysis,[9−14] sensing,[15−18] imaging,[19−22] and biomedicine.[23−27] For Ag (or Au) nanocrystals, the applications are largely based on their fascinating optical properties known as local surface plasmon resonance (LSPR).[28−31] To this end, both computational and experimental studies have shown that the shape of a nanocrystal plays the most important role in determining the number and position of LSPR modes. Thanks to the efforts from many research groups, a wide variety of methods have been developed for the synthesis of Ag nanocrystals with different shapes, including sphere, cube, octahedron, bar, bipyramid, plate, decahedron, rod, and wire.[32−40] Among them, polyhedrons with a single-crystal structure and enclosed by a mix of {100} and {111} facets in different proportions (e.g., cube, cuboctahedron, and octahedron) have gained particular interest due to their great potential as substrates for plasmonic sensing[41,42] and surface-enhanced Raman scattering (SERS);[40,43,44] as building blocks for self-assembly;[45,46] and as sacrificial templates for generating hollow structures made of other noble metals.[35,47] These Ag polyhedrons could readily be prepared using the polyol method developed by our group,[35] which has also been refined by Yang and other groups in conjunction with the concept of seed-mediated growth.[36]

Seed-mediated growth represents a simple and versatile route to noble-metal nanocrystals with controlled sizes and shapes. The concept of seed-mediated growth was initially conceived by Murphy and co-workers for the synthesis of Au nanorods from Au seeds[48] and by our group for the production of Ag nanowires from Pt seeds.[49] In recent years, this approach has been extended to other metals including Pd, Pt, Rh, and Cu, as well as their combinations.[34,40,50−54] As an advantage over conventional methods based on homogeneous nucleation, seed-mediated growth allows one to disentangle growth from nucleation, making it easier to control both the size and shape of a product by simply concentrating on the growth step. In the absence of a capping agent, the free energies of various facets of a Ag polyhedron increase in the order of $\gamma_{\{111\}} < \gamma_{\{100\}} < \gamma_{\{110\}}$. As such, when Ag cubes are employed as the seeds for growth in the absence of a capping agent, the {100} facets will be gradually replaced with the more stable {111} facets, leading to the formation of truncated cubes, cuboctahedrons, and finally octahedrons.[3,6,55] In the presence of a capping agent, the seeds can be directed to grow into nanocrystals with different shapes depending on the binding affinities of the capping agent for different types of facets. These arguments are valid for seeds

Received: October 25, 2011
Published: December 28, 2011

   dx.doi.org/10.1021/ja210047e | J. Am. Chem.Soc. 2012, 134, 1793−1801

with both cubic and cuboctahedral shapes. For example, it has been demonstrated that single-crystal seeds of Ag with a cuboctahedral shape could be directed to grow into octahedrons enclosed by {111} facets or cubes encased by {100} facets when sodium citrate or poly(vinylpyrrolidone) (PVP) was used as a capping agent while all other parameters were kept the same.[40] In these cases, the citrate ions and PVP bind most strongly to {111} and {100} facets, respectively, reducing their free energies and thus growth rates. In a sense, the binding of a capping agent can alter the free energies of various facets and even reverse their order. The facets expressed on the final product should be a manifestation of the order of free energies for different facets after the binding of capping agent has been taken into account.

Although previous studies have demonstrated the capabilities of various capping agents in generating Ag nanocrystals with different shapes,[40,56,57] there is no quantitative analysis of the explicit role played by a specific capping agent. Taking PVP as an example, up to this point, it is still not clear whether the initial concentration and molecular weight of this polymer will have a major impact on the shape evolution of a Ag nanocrystal. In this article, we conducted a set of experiments to achieve a quantitative understanding of the explicit role played by PVP in a seed-mediated synthesis. The experiments involved the use of Ag nanocubes as seeds in ethylene glycol (EG) at an elevated temperature, with $AgNO_3$ serving as a precursor to Ag and PVP of two molecular weights and in different initial concentrations serving as the capping agent. We found that well-defined polyhedrons ranging from cubes (with enlarged sizes relative to the seeds) to truncated cubes, cuboctahedrons, truncated octahedrons, and octahedrons could all be obtained depending on the initial concentration of PVP added to the reaction solution. We also derived the coverage density (ϕ) of PVP on Ag(100) surface by combining the results from two experiments. In the first experiment, we followed the growth of Ag cubic seeds at a fixed initial concentration (C_1) of PVP and found out the time (and thus the size of corresponding cubes) at which {111} facets started to appear on the cubes. In the second experiment, the same batch of Ag cubic seeds was allowed to grow at a set of initial concentrations of PVP to figure out at which concentration (C_2) {111} facets would start to appear on the cubic seeds at the very beginning of growth. We then calculated the coverage density of PVP on Ag(100) from the differences in concentration ($C_1 - C_2$) and total surface area of Ag cubes between these two samples. We compared the coverage densities for PVP with two different molecular weights (55 000 and 10 000 g/mol) and Ag cubic seeds of two different sizes (40 and 100 nm in edge length). To our knowledge, this work represents the first attempt for a quantitative analysis of the effect of a capping agent on the shape evolution and growth habit of noble-metal nanocrystals. The Ag polyhedrons with well-defined shapes and controllable sizes also allowed for a systematic study of their LSPR properties as a function of these two parameters.

2. EXPERIMENTAL SECTION

Chemicals and Materials. Ethylene glycol (EG, lot no. G32B27) was obtained from J. T. Baker. Silver trifluoroacetate (CF_3COOAg, ≥99.99%), silver nitrate ($AgNO_3$, 99+%), sodium hydrosulfide hydrate ($NaHS{\cdot}xH_2O$), hydrochloric acid (HCl, 37% in water), 1-methyl-2-pyrrolidinone (99%), and poly(vinylpyrrolidone) (PVP55 with $M_W \approx$ 55 000 and PVP10 with $M_W \approx$ 10 000) were all obtained from Sigma-Aldrich. Note that the molecular weights of a commercial PVP typically have a relatively broad distribution.[58,59] 1,4-Benzenedithiol (1,4-BDT, 98%) was purchased from Alfa Aesar. All aqueous solutions were prepared using deionized (DI) water with a resistivity of 18.2 MΩ·cm. All syntheses of Ag nanocrystals were carried out in 100 mL flasks with round bottom (ACE Glass).

Preparation of 40 nm Ag Cubes To Be Used as the Seeds. The 40 nm cubic seeds of Ag were prepared using a recently reported protocol with minor modifications.[58] In a typical synthesis, 20 mL of EG was added into a 100 mL flask and preheated under magnetic stirring in an oil bath set to 150 °C. Other reagents dissolved in EG were sequentially added into the flask using a pipet: 250 μL of NaHS solution (3 mM) was first added, and after 2 min, 2 mL of HCl (3 mM) was added, followed by 5 mL of PVP55 (20 mg/mL). After another 2 min, 1.5 mL of CF_3COOAg solution (282 mM) was added. During the entire process, the flask was capped with a glass stopper except during the addition of reagents. The 40 nm cubic seeds of Ag were obtained by quenching the reaction with an ice-water bath when the suspension had reached a brown color with a major LSPR peak around 435 nm. After centrifugation and being washed with acetone once and DI water twice, the seeds were redispersed in 2 mL of EG for further use. The particle concentration was 5.0×10^{12} particles/mL based on the concentration of Ag measured using inductively coupled plasma mass spectrometry (ICP-MS) and the particle size and shape determined by electron microscopy.

Preparation of 100 nm Ag Cubes To Be Used as the Seeds. The 100 nm cubic seeds of Ag were prepared using seed-mediated growth.[60] In a typical synthesis, 20 mL of EG was added into a 100 mL flask and heated in an oil bath at 150 °C under magnetic stirring. After 10 min, 6 mL of PVP55 solution (20 mg/mL, in EG) was added using a pipet. After another 10 min, 200 μL of the suspension of 40 nm Ag cubes (5.0×10^{12} particles/mL) in EG was introduced, followed by the addition of 4 mL of $AgNO_3$ solution (282 mM, in EG) using a pipet. The 100 nm cubic seeds of Ag were obtained by quenching the reaction with an ice-water bath when the major LSPR peak of the product had reached ~585 nm. The product was washed with acetone once and DI water twice and then redispersed in 0.5 mL of EG for further use. The particle concentration was 2.0×10^{12} particles/mL.

Seed-Mediated Growth for Ag Polyhedrons. In a standard synthesis, 15 mL of EG was added into a 100 mL flask and heated for 30 min under magnetic stirring in an oil bath set to 140 °C, and then 0.5 mL of the suspension of 40 or 100 nm Ag cubes in EG was introduced. After 2 min, 3 mL of PVP55 or PVP10 solution (in EG, with a specific concentration noted in the text) and 2 mL of $AgNO_3$ (564 mM, in EG) were simultaneously added at rates of 1.0 and 0.5 mL/min, respectively, using syringe pumps. The reaction time was counted immediately after the addition of $AgNO_3$ solution. Aliquots were taken at different time points of a synthesis using glass pipets and then quickly injected into cold acetone held in 1.5 mL centrifuge tubes. Additionally, a small amount (several drops) of the solution was taken with a glass pipet, diluted with DI water in a cuvette, and subjected to measurement of UV−vis spectrum. These procedures could be completed in 1 min, during which the Ag nanocrystals grew very little in size. All the final products were collected by centrifugation, followed by washing with acetone once and then DI water three times to remove excess reagents. The final products were dispersed in DI water for further characterizations.

Surface-Enhanced Raman Scattering (SERS) Measurements. The as-prepared samples were diluted with water to obtain aqueous suspensions with a particle concentration of 1.2×10^{11} particles/mL. For SERS measurements with 1,4-BDT as a probe molecule, the Ag nanocrystals were functionalized with a 1 mM ethanol solution of 1,4-BDT over a period of 2 h. Ethanol was used to wash the sample several times before the particles were redispersed in water to obtain a concentration of 1.2×10^{11} particles/mL. Sample cells were constructed by attaching the cap of a microcentrifuge tube to a glass slide. The cap served as a vessel for the liquid sample, and a glass coverslip (0.13−0.17 mm) was carefully placed on top to prevent solvent evaporation and to serve as a reference point from which the focal point was lowered to a depth of 0.2 mm into the sample.

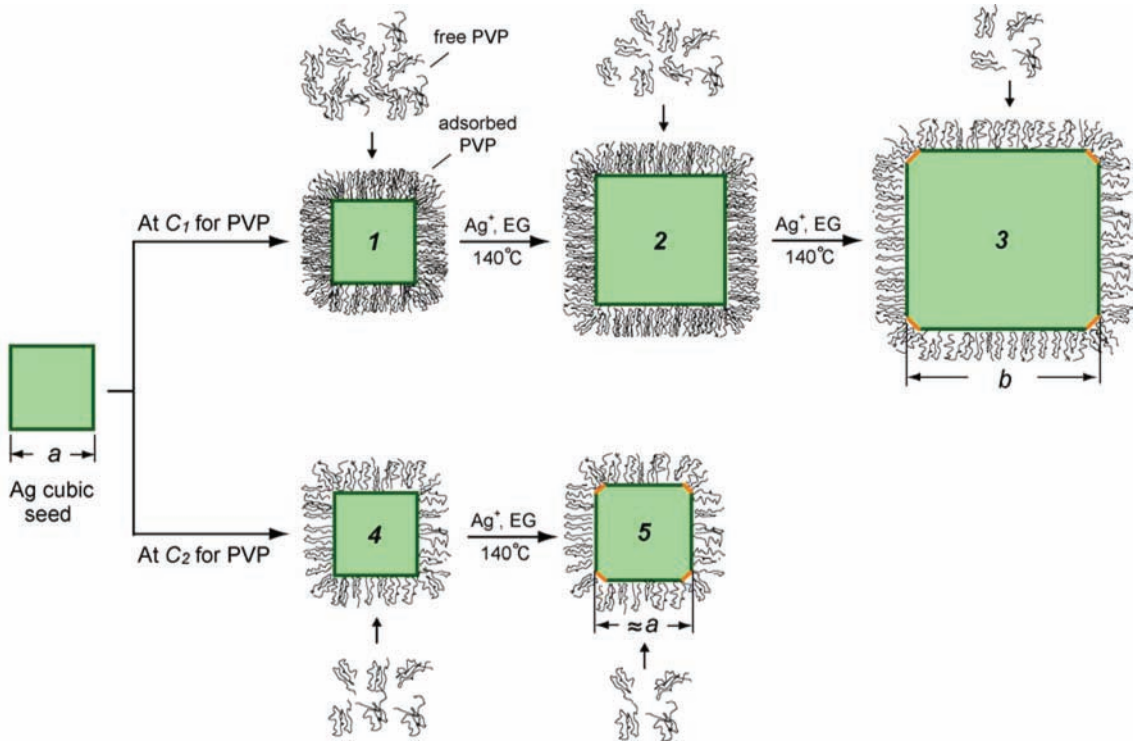

Figure 1. Schematic showing the growth of a Ag cubic seed with an edge length of a nm in the presence of PVP at a high concentration of C_1 and a critical concentration of C_2 ($C_1 > C_2$), respectively. At C_1, enough free PVP in the solution ensures surface adsorption and thus good passivation of the Ag(100) surface of the cubic seed (**1**), which can grow to a bigger cube (**2**), accompanied by reduction in PVP concentration due to its adsorption onto the newly formed Ag surface. Eventually, when the concentration of free PVP drops to a critical value (C_2), the PVP can no longer passivate the Ag(100) surface, the free energies of {100} and {111} facets become the same, and {111} facets start to appear on the surface, leading to the formation of a larger cube of b nm in size (**3**) with slight truncation at corners. Alternatively, when the initial concentration of PVP is reduced to the critical value (C_2), {111} facets start to appear on the surface of the cubic seed at the very beginning of growth, leading to the formation of a slightly truncated cube (**5**) with essentially the same size as the initial seed.

We employed the 1,4-BDT SERS peak at 1562 cm^{-1} (the strongest band in the spectra) to calculate the SERS EFs using the following equation[61]

$$\mathrm{EF} = (I_{\mathrm{SERS}} \times N_{\mathrm{bulk}})/(I_{\mathrm{bulk}} \times N_{\mathrm{SERS}}) \quad (1)$$

where I_{SERS} and I_{bulk} are the intensities of the same band for the SERS and ordinary spectra from a bulk sample, N_{bulk} is the number of molecules probed for a bulk sample, and N_{SERS} is the number of molecules probed in SERS. N_{bulk} was determined based on the Raman spectrum of an aqueous solution containing 0.1 M 1,4-BDT and 12 M NaOH and the focal volume (1.48 pL) of our Raman system. When determining N_{SERS}, we assumed that the 1,4-BDT molecules were adsorbed as a monolayer with a molecular footprint of 0.54 nm^2,[62] and surface areas of 3.4×10^4 and 1.9×10^4 nm^2 were used for a nanocube and a octahedron both of 75 nm in edge length based on SEM imaging.

Instrumentation. SEM images were captured using a Nova NanoSEM 230 field-emission microscope (FEI, Hillsboro, OR) operated at 15 kV. Transmission electron microscopy (TEM) images were taken using a Tecnai G2 Spirit Twin microscope (FEI, Hillsboro, OR) operated at 120 kV. The concentration of Ag was determined using an ICP-MS (Perkin-Elmer Elan DRC II ICP-MS) and then converted into the concentration of Ag nanocrystals once the particle size and shape had been determined by TEM and SEM imaging. The samples for ICP-MS were prepared by dissolving 10 μL of the suspension of Ag nanocrystals with 30 μL of concentrated HNO_3. The resultant solution was further diluted to the 100 ppb level for ICP-MS analysis. Extinction spectra of all the Ag nanocrystals were recorded using a UV−vis spectrometer (Varian, Cary 50). The SERS spectra were recorded using a Renishaw in Via confocal Raman spectrometer coupled to a Leica microscope with a 50× objective (N.A. = 0.90). The light source at 514 nm was generated from an argon cw laser and used with a holographic notch filter based on a grating of 1200 lines per mm. The backscattered Raman signals were collected on a thermoelectrically cooled (−60 °C) CCD detector. The SERS data were collected with $P_{\mathrm{laser}} \approx 2$ mW and $t = 30$ s. All data analyses were done with IGOR Pro software (Portland, OR).

3. RESULTS AND DISCUSSION

Quantitative Analysis of the Surface Coverage Density of PVP. Figure 1 schematically illustrates how to experimentally determine the coverage density (ϕ) of PVP on Ag(100) surface. As expected, PVP will adsorb onto the surface of Ag nanocrystals upon contacting each other, and the surface coverage density of PVP on a Ag nanocrystal is dependent on the concentration of free PVP in the solution. During the growth of Ag nanocrystals, the concentration of free PVP drops with time due to the increase in total surface area for the nanocrystals and thereby increase of surface-bound PVP. If the initial concentration (C_1) of PVP is high enough, there will be sufficient free PVP in the solution to maintain the coverage density of PVP on the surfaces of all Ag cubic seeds as they grow in size. In this case, the cubic seed (a nm in edge length) will grow in size as a function of time without experiencing any change to its shape (Figure 1, **1** to **2**). However, the growth will eventually lead the concentration of free PVP in the solution to drop to a critical level, at which surface passivation by PVP can no longer be maintained. At this point, the surface free energies of {100} facets and {111} facets will become the same and {111} facets will start to appear on the surface, leading to the

dx.doi.org/10.1021/ja210047e | J. Am. Chem.Soc. 2012, 134, 1793−1801

formation of a cube (b nm in edge length) with slight truncation at corners (Figure 1, **3**). Alternatively, one could gradually reduce the initial concentration of PVP used for a synthesis until a specific value (C_2) is reached, at which {111} facets will start to appear on the seed at the very beginning of growth (Figure 1, **4** to **5**).

Since the concentrations of free PVP and coverage densities of PVP on the Ag(100) surface should be the same for samples **3** and **5**, the coverage density can now be calculated from the differences in initial concentration of PVP and the total surface area (ΔS_{Ag})

$$\phi = (C_1 - C_2)\cdot V\cdot N_A/\Delta S_{Ag} \quad (2)$$

where V is the volume of the reaction solution that was 0.02 L for all of our experiments and N_A is Avogadro's number (6.02×10^{23}). ΔS_{Ag} equals the total number (1.0×10^{12}) of cubic seeds multiplied by $6(b^2 - a^2)$ nm^2, the increase in surface area between the two different cubes.

Derivation of Surface Coverage for PVP55 and 40 nm Cubic Seeds. We started our measurements with Ag cubes of 40 nm in edge length as the seeds and PVP55 of various molar concentrations as the capping agent. Here the concentration of PVP was calculated in terms of the repeating unit of PVP with a molecular weight of 111 g/mol. As shown by the SEM and TEM images in Figure S1(A) of the Supporting Information, the cubic seeds were 40 ± 1 nm in edge length, together with uniform distributions for both size and shape. The initial concentration (C_1) of PVP55 in the solution was first set to 1.0 mM. At t = 5 and 10 min, the 40 nm cubic seeds had evolved into Ag cubes with average edge lengths of 55 and 75 nm, respectively, as shown in Figure 2, A and B. The corners of these cubes were even slightly sharper than those of the original cubic seeds (with the radii of curvature at corner sites being approximately 6, 4, and 4 nm, respectively, for the 40 nm seed, 55 nm cube, and 75 nm cube, see Figure S2). These results imply that the PVP55 could effectively passivate the Ag(100) surface via adsorption, leading to the formation of Ag nanocubes enclosed by {100} facets. In this case, the cubic seed was merely enlarged in size with almost no development of {111} facets. However, as the reaction was prolonged to t = 20 min (Figure 2C), we obtained Ag nanocubes with slight truncation and thus formation of eight {111} facets at the corners.

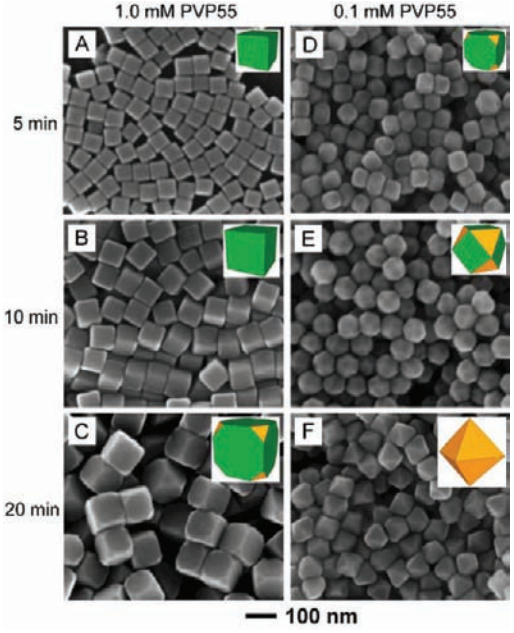

Figure 2. SEM images of Ag polyhedrons grown from 40 nm cubic seeds in the presence of (A–C) 1.0 mM and (D–F) 0.1 mM PVP55, respectively, as the capping agent. The samples were collected from the reaction solutions at different time points: (A, D) 5 min, (B, E) 10 min, and (C, F) 20 min. The inset shows the corresponding 3D model for each type of polyhedron.

When the reaction time was further extended, truncated cubes, truncated octahedrons, and octahedrons were observed at t = 25, 45, and 75 min, respectively (Figure S3). During this period of time (20–75 min), the total area of {111} facets was constantly enlarged at the expense of {100} facets, which eventually disappeared. When {111} facets started to appear at t = 20 min, it implies that the surface of nanocrystals could no longer be passivated by PVP and therefore {111} facets would start to grow at the expense of {100} facets. At t = 75 min, a perfect Ag octahedron with an edge length of 220 nm was developed (Figure S3C), and no additional growth was observed thereafter for the octahedrons due to the self-limiting feature of {111} facets.[63] At the same time, irregular particles started to appear in the product (Figure S3D) due to homogeneous nucleation and growth. When we increased the initial molar concentration of PVP from 1.0 to 2.0 mM, 130 nm sharp cubes with no truncation at corners were obtained at t = 20 min (Figure S4), confirming our assumption that the presence of sufficient PVP55 in the solution was a key parameter in maintaining good passivation for {100} facets and thus their dominance over {111} facets during the growth process.

The result in Figure 2C indicates that the 40 nm cubic seed (a = 40 nm) would grow into a cube (b = 120 nm) with slight corner truncation at C_1 = 1.0 mM and t = 20 min. In order to obtain the concentration of PVP at which {111} facets will start to appear at corners from the very beginning and thus calculate ϕ, we conducted a set of syntheses with decreasing initial concentrations for PVP. Aliquots were taken from the reaction solutions at a very early stage (t = 5 min) and analyzed by SEM to monitor the growth process. Interestingly, when the concentration of PVP was reduced to a critical value (C_2) of 0.1 mM, {111} facets would start to appear from the very beginning (Figure 2D). Further growth of these truncated cubes eventually led to the formation of cuboctahedrons (Figure 2E) and perfect octahedrons (Figure 2F). These results imply that C_2 was likely around 0.1 mM for PVP55 and 40 nm seeds. From these data and eq 2, the value of ϕ for PVP55 and 40 nm seeds was calculated to be approximately 140 repeating units per nm^2. Since the area occupied by a PVP monomer (i.e., *N*-vinypyrrolidone) is around 0.21 nm^2 (see Figure S5 for detailed calculation), the number of repeating units in each segment of PVP folded on the Ag surface is approximately 29.

In an ideal situation where growth is limited to the [100] directions only, the edge lengths of the resultant octahedron and the cubic seed should be related by a factor of 2.12.[64] From the TEM images (Figure S6), we found that the average edge length (75 nm) of the octahedrons shown in Figure 2F was 8.5% smaller than the edge length of 82 nm expected for octahedrons grown from 40 nm cubes under an ideal situation. This small discrepancy can be attributed to the slight truncation at corners for the initial cubic seeds (see Figure S7).

By further reducing the initial molar concentration of PVP to the range of 0.02−0.1 mM, we found that the results were more or less similar to what was observed for C_2 = 0.1 mM (data not shown). However, when the concentration was below 0.02 mM or no PVP55 was added into the reaction solution, Ag cubes with different degrees of truncation at corners and cuboctahedrons with round corners (Figure S8) were observed at t = 5 and 10 min, respectively. In these cases, there was not sufficient PVP to passivate the newly formed Ag(100) surface on Ag nanocrystals. The new morphologies were likely products of preferential growth of Ag on those sites where the surfaces were poorly covered by PVP.[65]

To better understand how PVP binds to the {100} and {111} facets, we obtained SERS spectra of PVP55 adsorbed on the surfaces of Ag nanocubes enclosed by {100} facets (shown in Figure 2B) and Ag octahedrons enclosed by {111} facets (shown in Figure 2F). Figure 3A shows the SERS spectra

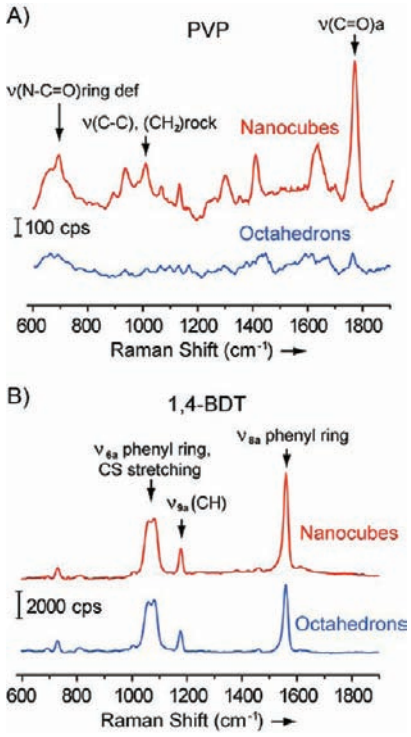

Figure 3. Solution-phase SERS spectra recorded from (A) as-prepared Ag nanocubes (Figure 2B) and octahedrons (Figure 2F) prepared in the presence of PVP and (B) the same samples of nanocubes and octahedrons after their surfaces had been functionalized with 1,4-BDT. Band assignments for PVP and 1,4-BDT are labeled above the peaks. All samples were suspended in water, and the suspensions had roughly the same particle concentration. cps = counts per second.

recorded from aqueous suspensions with roughly the same particle concentration (1.2×10^{11} particles/mL). Clearly, the intensity of characteristic C═O peak[66,67] for PVP molecules on the Ag nanocubes was much higher than those on the Ag octahedrons, implying a higher surface coverage density of PVP on the nanocubes. Figure 3B shows SERS spectra recorded from the same samples of Ag nanocubes and octahedrons after their surfaces had been functionalized with monolayers of 1,4-BDT.[43,68] Based on the phenyl ring stretching mode at 1562 cm^{-1}, the enhancement factors (EFs) were estimated to be 2.3×10^5 and 2.7×10^5 for the nanocubes and octahedrons, respectively, based on eq 1. Since the Ag nanocubes and octahedrons had similar SERS EFs for 1,4-BDT, the stronger intensity of PVP SERS peak from the Ag nanocubes could be attributed to a higher coverage density of PVP on the surface of Ag nanocubes than Ag octahedrons.

The Effect of PVP Molecular Weight on the Surface Coverage Density. Besides the concentration, the molecular weight of PVP was also found to have an impact on the shape evolution of a Ag nanocrystal. To single out the role of molecular weight, we repeated the experiments performed for PVP55 under similar conditions (e.g., by using the same type and concentration of seeds, precursor, temperature, and PVP concentration) except for the use of PVP with a molecular weight of 10 000 (PVP10). At C_1 = 1.0 mM, 65, 90, and 130 nm sharp cubes were obtained at t = 5, 10, and 20 min, respectively (Figure 4, A−C), indicating that {100} facets were

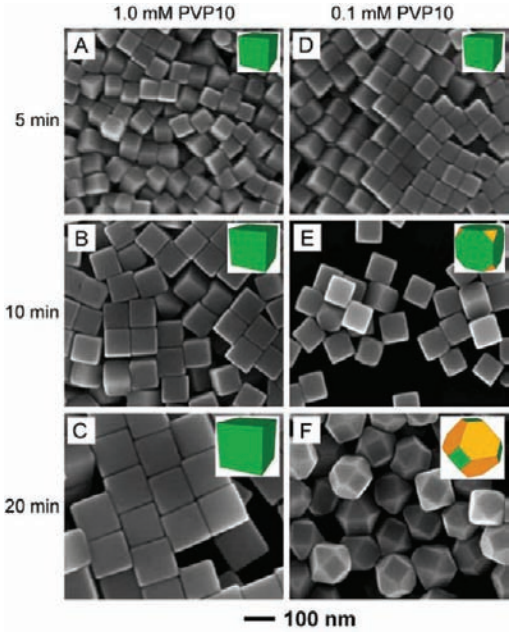

Figure 4. SEM images of Ag polyhedrons grown from 40 nm cubic seeds in the presence of (A−C) 1.0 mM and (D−F) 0.1 mM PVP10 as the capping agent. The samples were collected from the reaction solutions at different reaction times: (A, D) 5 min, (B, E) 10 min, and (C, F) 20 min. The inset shows the corresponding 3D model for each type of polyhedron.

lower in energy than {111} facets at least until t = 20 min. Note that {111} facets already started to appear at this time point when PVP55 was used at the same concentration. When C_1 was reduced to 0.1 mM, sharp cubes, slightly truncated cubes, and truncated octahedrons (Figure 4, D−F), were obtained at t = 5, 10, and 20 min, respectively. In these cases, there were still {100} facets on the surface at t = 20 min, while they had completely disappeared in the case of PVP55. These results indicate that PVP10 was more effective in reducing the surface free energy of Ag(100) than PVP55 when they were used at the same concentration in terms of repeating unit. The difference might be caused by the larger size and thus steric effect of PVP55 that tended to make it harder for the polymer chains to adsorb and pack on the surface of a Ag nanocrystal. Interestingly, we found that the cubic seeds grew into round particles at t = 10 min when 0.1 mM 1-methyl-2-pyrrolidinone, a monomer analogue of PVP, was used to replace the PVP10, with other reaction conditions being kept the same (see Figure

dx.doi.org/10.1021/ja210047e | J. Am. Chem.Soc. 2012, 134, 1793−1801

S9). This result is similar to the case when no PVP was added into the reaction solution. The lack of a polyvalency effect for the monomer analogue of PVP might be responsible for the reduction in binding affinity for the {100} facets and thus the disappearance of {100} facets during growth.[69,70]

To quantitatively understand how more effective PVP10 was in reducing the surface free energy of Ag(100), we also derived the value of ϕ for PVP10 and 40 nm cubic seeds. The images in Figure 4 suggest that the cubic seed with a = 40 nm started to show truncation at corners once its size had grown to b = 85 nm by t = 10 min at C_1 = 0.1 mM (Figure 4E). To obtain C_2 and thus calculate the ϕ of PVP10, we also performed syntheses at gradually decreasing concentrations of PVP with other parameters being kept the same. Results similar to what were shown in Figure 2, D–F, were observed when the initial concentration of PVP10 was reduced to 0.015 mM (data not shown). This observation indicates that C_2 was 0.015 mM for PVP10 and 40 nm cubic seeds. Using the same method developed for PVP55, the value of ϕ was calculated to be approximately 30 repeating units per nm^2 for PVP10 and 40 nm cubic seeds. Note that the value of ϕ for PVP10 was only about one-fourth of that for PVP55, indicating that PVP with a lower molecular weight was more effective in passivating the Ag(100) surface likely due to more efficient adsorption and packing.

The Effect of Seed Size on Surface Coverage Density. To examine the effect of seed size on ϕ, we conducted a set of syntheses by replacing the 40 nm Ag cubes with 100 nm Ag cubes as the seeds while all other parameters were kept the same except for the PVP concentration. Figure S1B shows SEM and TEM images of the 100 nm cubic seeds, which had sharp corners and were 100 ± 2 nm in edge length. We first used PVP55 as a capping agent in the syntheses. As shown in Figure 5, A–C, for C_1 = 2.5 mM, 130, 190 nm sharp cubes and 240 nm slightly truncated cubes at t = 15, 45, and 80 min, respectively, were obtained. The cubic seed with a = 100 nm started to show truncation at t = 80 min when its edge length became b = 240 nm (Figure 5C). We then gradually reduced the initial molar concentration of PVP55 and found that slightly truncated cubes of 120 nm in edge length were formed at t = 15 min when the PVP concentration was reduced to 0.3 mM. As the reaction proceeded, truncated octahedrons and octahedrons (Figure 5, E and F) were formed at t = 45 and 80 min, respectively. The edge length (210 nm, as shown in Figure 5F) of the octahedron was longer than that of the 100 nm cubic seed by a factor of 2.10, indicating that the octahedron was grown from the cubic seed under a more or less ideal situation. These results indicate that C_2 was 0.3 mM for this system. According to eq 2, the value of ϕ for PVP55 and 100 nm seeds became approximately 100 repeating units per nm^2, which was very close to what was derived for 40 nm cubic seeds.

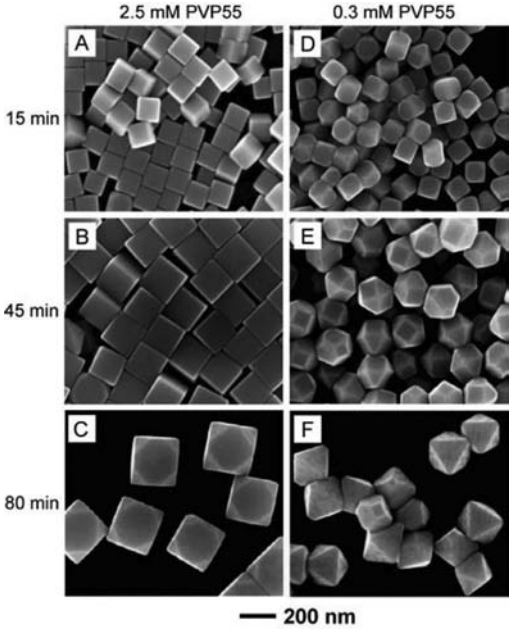

Figure 5. SEM images of Ag polyhedrons grown from 100 nm cubic seeds in the presence of (A–C) 2.5 mM and (D–F) 0.3 mM PVP55 as the capping agent. The samples were collected from the reaction solutions at different reaction times: (A, D) 15 min, (B, E) 45 min, and (C, F) 80 min.

To obtain ϕ for PVP10 and 100 nm cubic seeds, we also performed a set of experiments under the same conditions as above, except for the use of PVP10 as a capping agent. At C_1 = 2.5 mM, 125, 200, and 275 nm sharp cubes (Figure 6, A–C) were obtained at t = 15, 45, and 80 min, respectively. When C_1 was reduced to 0.3 mM, 120 nm sharp cubes, 190 nm truncated cubes, and 260 nm cuboctahedrons (Figure 6, D–F) were formed at t = 15, 45, and 80 min, respectively. By gradually reducing the initial concentration of PVP10, the cubes started to show truncation at t = 0 min when it was reduced to C_2 = 0.03 mM (data not shown). Accordingly, the ϕ value for PVP10 and 100 nm cubic seeds was calculated to be approximately 20 repeating units per nm^2. The values of ϕ for PVP55 and PVP10 adsorbed on the 100 nm cubic seeds were of the same orders of magnitude as the values derived for the 40 nm cubic seeds. Taken together, it is clear that ϕ has a

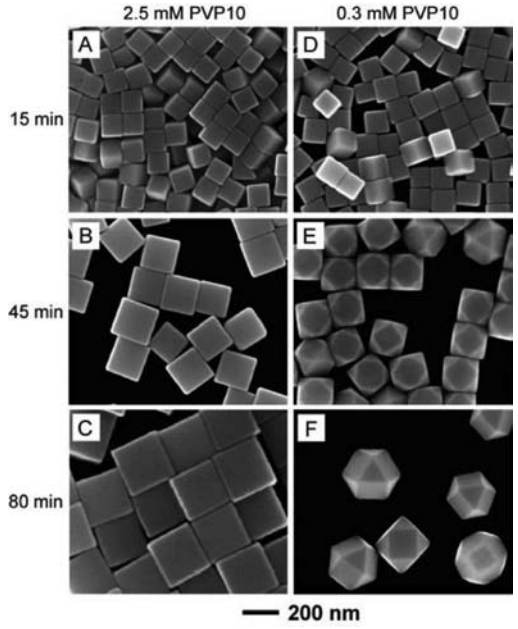

Figure 6. SEM images of Ag polyhedrons grown from 100 nm cubic seeds in the presence of (A–C) 2.5 mM and (D–F) 0.3 mM PVP10 as the capping agent. The samples were collected from the reaction solutions at different reaction times: (A, D) 15 min, (B, E) 45 min, and (C, F) 80 min, respectively.

dx.doi.org/10.1021/ja210047e | J. Am. Chem.Soc. 2012, 134, 1793–1801

much stronger dependence on the molecular weight of PVP than the size of the cubic seeds.

Reaction Kinetics of the Seed-Mediated Growth. We also studied the reaction kinetics to better understand the roles played by both the concentration and molecular weight of PVP in shape evolution during the growth of Ag cubic seeds. We first plotted the sizes (L) of Ag nanocrystals as a function of reaction time (t). Here L was defined as the distance between two opposite {100} facets as illustrated in Figure S10. When PVP was used as a capping agent and 40 nm cubes as the seeds (Figures 2 and 4), there was a more or less linear relationship between the size of Ag nanocrystals and reaction time for both PVP55 and PVP10 at two different concentrations (Figure 7A).

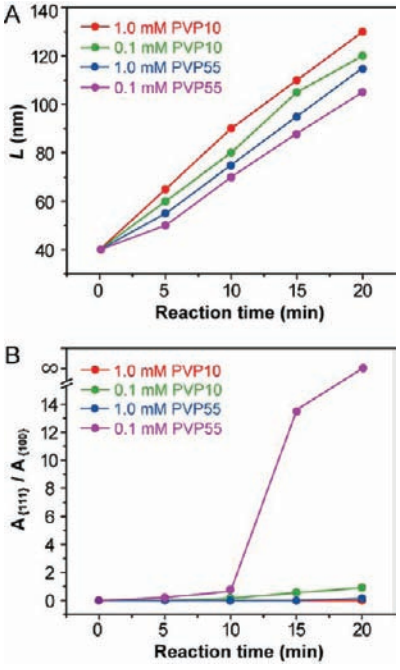

Figure 7. Plots of (A) the size (L) and (B) the ratio between areas of {111} and {100} facets (denoted as $A_{\{111\}}$ and $A_{\{100\}}$, respectively) for the Ag nanocrystals shown in Figures 2 and 4 as a function of reaction time.

Their slopes fell into the range of 3.1−4.1 nm/min, which corresponded to the growth rate along the [100] directions. The nanocrystals obtained at a higher concentration of PVP were always slightly larger than those obtained at a lower concentration of PVP with the same molecular weight at a specific reaction time. Meanwhile, the nanocrystals obtained with PVP10 were slightly larger in size than those prepared with PVP55 at the same concentration and reaction time. These data also imply that more Ag atoms were added onto the seeds when PVP at a higher concentration or with a lower molecule weight was used in the synthesis. These results can be explained by the coordination effect of PVP with Ag^+ ions (thus effectively lowering the reduction potential of Ag^+). The same phenomenon was also observed when citrate was used as a capping agent for Ag nanoplates.[71] In addition, Ag^+−PVP10 complex may form more easily than Ag^+−PVP55 due to a weaker steric effect for the shorter polymer chains. We also plotted the ratio between the areas of {111} and {100} facets expressed on the surface as a function of reaction time. As shown in Figure 7B, the ratio increased rapidly as the reaction proceeded when PVP55 was used at a concentration of 0.1 mM, which was much faster than what we observed for 0.1 mM PVP10.

A similar trend was also observed when 100 nm cubes were used as the seeds and PVP in different molecular weights and concentrations as the capping agent (Figures S11). The growth rate (1.9−2.5 nm/min) for the syntheses with 100 nm seeds was roughly two times lower than the rate (3.1−4.1 nm/min) obtained for the 40 nm seeds. This can be explained by the fact that a larger seed has a larger surface area and thus requires more Ag atoms to achieve a growth rate the same as the case with a smaller seed.

Optical Properties of the Ag Nanocrystals. The Ag nanocrystals with controlled sizes and well-defined shapes allowed us to systematically investigate the effects of size and shape on LSPR. Figure 8A shows normalized UV−vis spectra

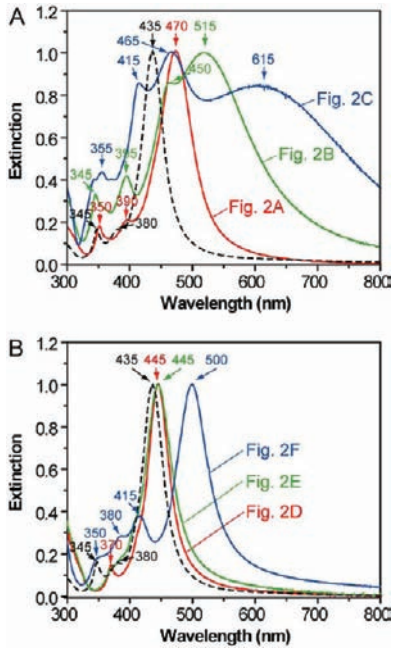

Figure 8. Normalized UV−vis spectra of samples shown in Figure 2 (as marked on the spectra). Dashed curves correspond to UV−vis spectra of the 40 nm Ag cubes serving as the seeds. The peak positions are labeled on each spectrum, and their assignments can be found in the text.

recorded from aqueous suspensions of the Ag nanocrystals shown in Figure 2, A−C. The major LSPR peaks displayed a constant red-shift from 435 to 470, 515, and 615 nm as the size of nanocrystals increased. Three LSPR peaks, which are dipole resonance modes, were present for the 50 nm cubes (Figure 2A), while four peaks, including a small shoulder at ~450 nm (next to the primary LSPR peak, a quadrupole resonance mode), can be resolved for the 70 nm cubes (Figure 2B). These observations are consistent with the characteristic dipole and quadrupole resonance peaks for Ag cubes at these sizes.[36,72] The 120 nm truncated Ag cubes (Figure 2C) showed relatively broad LSPR peaks, which might be attributed to their large sizes and thus the involvement of multipode excitations in addition to dipole excitation.[36,72]

Figure 8B shows UV−vis spectra of the Ag nanocrystals shown in Figure 2, D−F. We found that the major LSPR peak was red-shifted very little from 435 to 445 nm at the beginning of the reaction, and the truncated cubes and cuboctahedrons

dx.doi.org/10.1021/ja210047e | J. Am. Chem.Soc. 2012, 134, 1793−1801

showed major LSPR peaks at the sample position of 445 nm. In comparison with the cubic seeds, there are only two peaks for the truncated cubes, with the peak observed at ~380 nm for the cubic seeds disappearing in the spectra of the truncated cubes. For the spectrum of cuboctahedrons, both peaks located at ~345 and 380 nm disappeared, mainly because a cuboctahedron has higher symmetry than a cube. It is interesting to note that there were four LSPR peaks for the Ag octahedron with an average edge length of 75 nm (Figure 2F), including three weak peaks located at 350, 380, and 415 nm, and one primary peak at 500 nm corresponding to one of the dipole modes.[40]

The LSPR peaks of Ag nanocrystals with larger sizes (100–300 nm, as shown in Figure 5) were relatively broad and thus less distinguishable (Figure S12). In practice, one can obtain Ag nanocrystals with a specific morphology and size by continuously monitoring changes to the UV–vis spectra taken at different reaction stages.

4. CONCLUSION

We have systematically investigated the role of PVP as a capping agent in controlling the shape evolution of Ag nanocrystals during a seed-mediated synthesis. It can be concluded that the coverage density of PVP adsorbed on the surface of a Ag nanocrystal plays a pivotal role in determining the surface free energies of Ag(100) and Ag(111) facets and thus the formation of nanocrystals with different shapes. We have also obtained the critical concentration of PVP in the solution and the coverage density of PVP on the surface, at which the order of free energies between Ag(100) and Ag(111) are reversed. Our results indicate that PVP with a relatively lower molecular weight was more effective in reducing the free energy of Ag(100) via surface adsorption than PVP with a higher molecular weight. By simply controlling the initial concentration of PVP added into a reaction solution, a series of Ag polyhedrons from enlarged cubes to truncated cubes, cuboctahedrons, truncated octahedrons, and octahedrons could all be easily obtained from cubic seeds. This work not only advances our understanding of the role played by PVP in controlling the shape evolution of Ag nanocrystals but also allows us to investigate the effects of both size and shape on the LSPR properties. The quantitative analysis reported in this article could also be extended to other systems involving different types of seeds and/or capping agents.

■ ASSOCIATED CONTENT

Supporting Information

SEM images of the 40 and 100 nm cubic seeds of Ag; curvature estimation for corner sites of the 40 nm seeds and cubes shown in Figure 2A and B; SEM images of Ag nanocrystals grown from the 40 nm cubic seeds with 1.0 mM PVP55 at t = 25, 45, 75, and 90 min, with 2.0 mM PVP55 at t = 5 and 20 min, without adding any PVP at t = 5 and 10 min, and with 0.1 mM 1-methyl-2-pyrrolidinone at t = 5 and 10 min; schematic drawing of a PVP monomer (*N*-vinypyrrolidone); TEM images of the Ag nanocrystals shown in Figure 2, D–F; a schematic showing how the size of the final octahedron is determined by the size of a slightly truncated cubic seed and how to define the size (L) of different Ag polyhedrons; plots of the size and the ratio between areas of {111} and {100} facets for the polyhedrons shown in Figures 5 and 6 as a function of reaction time; UV–vis spectra taken from products of the syntheses shown in Figure 5. This material is available free of charge via the Internet at http://pubs.acs.org.

■ AUTHOR INFORMATION

Corresponding Author

younan.xia@bme.gatech.edu

Present Address

[⊥]The Wallace H. Coulter Department of Biomedical Engineering, Georgia Institute of Technology and Emory University Medical School, and School of Chemistry and Biochemistry, Georgia Institute of Technology, Atlanta, Georgia 30332, United States.

Author Contributions

[§]These authors contributed equally to this work.

■ ACKNOWLEDGMENTS

This work was supported in part by the NSF (DMR-1104614) and NIH (R01 CA13852701). As a jointly supervised Ph.D. student from Xiamen University, X.X. was also partially supported by a Fellowship from the China Scholarship Council.

■ REFERENCES

(1) Jain, P. K.; Huang, X.; El-Sayed, I. H.; El-Sayed, M. A. *Acc. Chem. Res.* **2008**, *41*, 1578–1586.
(2) Murphy, C. J.; Sau, T. K.; Gole, A. M.; Orendorff, C. J.; Gao, J.; Gou, L.; Hunyadi, S. E.; Li, T. *J. Phys. Chem. B* **2005**, *109*, 13857–13870.
(3) Xia, Y.; Xiong, Y.; Lim, B.; Skrabalak, S. E. *Angew. Chem., Int. Ed.* **2009**, *48*, 60–103.
(4) Park, J.; Joo, J.; Kwon, S. G.; Jang, Y.; Hyeon, T. *Angew. Chem., Int. Ed.* **2007**, *46*, 4630–4660.
(5) Millstone, J. E.; Hurst, S. J.; Métraux, G. S.; Cutler, J. I.; Mirkin, C. A. *Small* **2009**, *5*, 646–664.
(6) Tao, A. R.; Habas, S.; Yang, P. *Small* **2008**, *4*, 310–325.
(7) Talapin, D. V.; Lee, J.-S.; Kovalenko, M. V.; Shevchenko, E. V. *Chem. Rev.* **2010**, *110*, 389–458.
(8) Daniel, M.-C.; Astruc, D. *Chem. Rev.* **2004**, *104*, 293–346.
(9) Narayanan, R.; El-Sayed, M. A. *Nano Lett.* **2004**, *4*, 1343–1348.
(10) Tian, N.; Zhou, Z.; Sun, S.; Ding, Y.; Wang, Z. *Science* **2007**, *316*, 732–735.
(11) Zhang, J.; Sasaki, K.; Sutter, E.; Adzic, R. R. *Science* **2007**, *315*, 220–222.
(12) Joo, S. H.; Park, J. Y.; Tsung, C. K.; Yamada, Y.; Yang, P.; Somorjai, G. A. *Nat. Mater.* **2009**, *8*, 126–131.
(13) Peng, Z.; Yang, H. *Nano Today* **2009**, *4*, 143–164.
(14) Zhang, J.; Yang, H. Z.; Fang, J. Y.; Zou, S. Z. *Nano Lett.* **2010**, *10*, 638–644.
(15) Elghanian, R.; Storhoff, J. J.; Mucic, R. C.; Letsinger, R. L.; Mirkin, C. A. *Science* **1997**, *277*, 1078–1081.
(16) Rosi, N. L.; Mirkin, C. A. *Chem. Rev.* **2005**, *105*, 1547–1562.
(17) Haes, A. J.; Haynes, C. L.; McFarland, A. D.; Schatz, G. C.; Van Duyne, R. P.; Zou, S. *MRS Bull.* **2005**, *30*, 368–375.
(18) Willets, K. A.; Van Duyne, R. P. *Annu. Rev. Phys. Chem.* **2007**, *58*, 267–297.
(19) Loo, C.; Lowery, A.; Halas, N.; West, J.; Drezek, R. *Nano Lett.* **2005**, *5*, 709–711.
(20) Yang, X.; Skrabalak, S. E.; Li, Z.-Y.; Xia, Y.; Wang, L. V. *Nano Lett.* **2007**, *7*, 3798–3802.
(21) Qian, X. M.; Peng, X. H.; Ansari, D. O.; Yin-Goen, Q.; Chen, G. Z.; Shin, D. M.; Yang, L.; Young, A. N.; Wang, M. D.; Nie, S. M. *Nat. Biotechnol.* **2008**, *26*, 83–90.
(22) Lal, S.; Clare, S. E.; Halas, N. J. *Acc. Chem. Res.* **2008**, *41*, 1842–1851.
(23) Seo, W. S.; Lee, J. H.; Sun, X. M.; Suzuki, Y.; Mann, D.; Liu, Z.; Terashima, M.; Yang, P. C.; McConnell, M. V.; Nishimura, D. G.; Dai, H. J. *Nat. Mater.* **2006**, *5*, 971–976.
(24) Xie, J.; Xu, C.; Kohler, N.; Hou, Y.; Sun, S. *Adv. Mater.* **2007**, *19*, 3163–3166.

(25) Gao, J. H.; Liang, G. L.; Zhang, B.; Kuang, Y.; Zhang, X. X.; Xu, B. *J. Am. Chem. Soc.* **2007**, *129*, 1428−1433.
(26) Peng, H.-I.; Strohsahl, C. M.; Leach, K. E.; Krauss, T. D.; Miller, B. L. *ACS Nano* **2009**, *3*, 2265−2273.
(27) Xia, Y.; Li, W.; Cobley, C. M.; Chen, J.; Xia, X.; Zhang, Q.; Yang, M.; Cho, E. C.; Brown, P. K. *Acc. Chem. Res.* **2011**, *44*, 914−924.
(28) Kelly, K. L.; Coronado, E.; Zhao, L. L.; Schatz, G. C. *J. Phys. Chem. B* **2003**, *107*, 668−677.
(29) Sosa, I. O.; Noguez, C.; Barrera, R. G. *J. Phys. Chem. B* **2003**, *107*, 6269−6275.
(30) Jensen, T. R.; Malinsky, M. D.; Haynes, C. L.; Van Duyne, R. P. *J. Phys. Chem. B* **2000**, *104*, 10549−10556.
(31) El-Sayed, M. A. *Acc. Chem. Res.* **2001**, *34*, 257−264.
(32) Rycenga, M.; Cobley, C. M.; Zeng, J.; Li, W.; Moran, C. H.; Zhang, Q.; Qin, D.; Xia, Y. *Chem. Rev.* **2011**, *111*, 3669−3712.
(33) Jin, R.; Cao, Y.; Mirkin, C. A.; Kelly, K. L.; Schatz, G. C.; Zheng, J. G. *Science* **2001**, *294*, 1901−1903.
(34) Jana, N. R.; Gearheart, L.; Murphy, C. J. *Chem. Commun.* **2001**, 617−618.
(35) Sun, Y.; Xia, Y. *Science* **2002**, *298*, 2176−2179.
(36) Tao, A. R.; Sinsermsuksakul, P.; Yang, P. *Angew. Chem., Int. Ed.* **2006**, *45*, 4579−4601.
(37) Wiley, B.; Sun, Y.; Xia, Y. *Acc. Chem. Res.* **2007**, *40*, 1067−1076.
(38) Pietrobon, B.; Kitaev, V. *Chem. Mater.* **2008**, *20*, 5186−5190.
(39) Zhang, J.; Li, S.; Wu, J.; Schatz, G. C.; Mirkin, C. A. *Angew. Chem., Int. Ed.* **2009**, *48*, 7787−7791.
(40) Zeng, J.; Zheng, Y.; Rycenga, M.; Tao, J.; Li, Z. Y.; Zhang, Q.; Zhu, Y.; Xia, Y. *J. Am. Chem. Soc.* **2010**, *132*, 8552−8553.
(41) Mulvihill, M.; Tao, A.; Benjauthrit, K.; Arnold, J.; Yang, P. *Angew. Chem., Int. Ed.* **2008**, *47*, 6456−6460.
(42) Galush, W. J.; Shelby, S. A.; Mulvihill, M. J.; Tao, A.; Yang, P.; Groves, J. T. *Nano Lett.* **2009**, *9*, 2077−2082.
(43) Rycenga, M.; Xia, X.; Moran, C.; Zhou, F.; Qin, D.; Li, Z.-Y.; Xia, Y. *Angew. Chem., Int. Ed.* **2011**, *50*, 5473−5477.
(44) McLellan, J. M.; Li, Z. Y.; Siekkinen, A. R.; Xia, Y. *Nano Lett.* **2007**, *7*, 1013−1017.
(45) Tao, A. R.; Sinsermsuksakul, P.; Yang, P. *Nat. Nanotech.* **2007**, *2*, 435−440.
(46) Rycenga, M.; McLellan, J. M.; Xia, Y. *Adv. Mater.* **2008**, *20*, 2416−2420.
(47) Skrabalak, S. E; Au, L.; Li, X.; Xia, Y. *Nat. Protoc.* **2007**, *2*, 2182−2190.
(48) Jana, N. R.; Gearheart, L.; Murphy, C. J. *J. Phys. Chem. B* **2001**, *105*, 4065−4067.
(49) Sun, Y.; Gates, B.; Mayers, B.; Xia, Y. *Nano Lett.* **2002**, *2*, 165−168.
(50) Habas, S. E.; Lee, H.; Radmilovic, V.; Somorjai, G. A.; Yang, P. *Nat. Mater.* **2007**, *6*, 692−697.
(51) Xue, C.; Millstone, J. E.; Li, S.; Mirkin, C. A. *Angew. Chem., Int. Ed.* **2007**, *46*, 8436−8439.
(52) Fan, F.-R.; Liu, D.-Y.; Wu, Y.; Duan, S.; Xie, Z.-X.; Jiang, Z.-Y.; Tian, Z.-Q. *J. Am. Chem. Soc.* **2008**, *130*, 6949−6951.
(53) Lim, B.; Jiang, M.; Camargo, P. H. C.; Cho, E. C.; Tao, J.; Lu, X.; Zhu, Y.; Xia, Y. *Science* **2009**, *324*, 1302−1305.
(54) Chen, Y.-H.; Hung, H.-H.; Huang, M. H. *J. Am. Chem. Soc.* **2009**, *131*, 9114−9121.
(55) Vitos, L.; Ruban, A. V.; Skriver, H. L.; Kollar, J. *Surf. Sci.* **1998**, *411*, 186−202.
(56) Zhang, Q.; Hu, Y.; Guo, S.; Goebl, J.; Yin, Y. *Nano Lett.* **2010**, *10*, 5037−5042.
(57) Zeng, J.; Xia, X.; Rycenga, M.; Henneghan, P.; Li, Q.; Xia, Y. *Angew. Chem., Int. Ed.* **2011**, *50*, 244−249.
(58) Zeng, X. M.; Martin, G. P.; Marriott, C. *Int. J. Pharm.* **2001**, *218*, 63−73.
(59) *Handbook of Pharmaceutical Excipients*; Wade, A., Weller, P. J., Eds.; Pharmaceutical Press: London, U.K., 1994; pp 392−399.
(60) Zhang, Q.; Li, W.; Moran, C.; Zeng, J.; Chen, J.; Wen, L. P.; Xia, Y. *J. Am. Chem. Soc.* **2010**, *132*, 11372−11378.
(61) McFarland, A. D; Young, M. A.; Dieringer, J. A.; Van Duyne, R. P. *J. Phys. Chem. B* **2005**, *109*, 11279−11285.
(62) Cho, S. H; Han, H. S.; Jang, D. J.; Kim, K.; Kim, M. S. *J. Phys. Chem.* **1995**, *99*, 10594−10599.
(63) Xia, X.; Zeng, J.; McDearmon, B.; Zheng, Y.; Li, Q.; Xia, Y. *Angew. Chem., Int. Ed.* **2011**, *50*, 12542−12546.
(64) Tsuji, M.; Maeda, Y.; Hikino, S.; Kumagai, H.; Matsunaga, M.; Matsuo, R.; Tang, X.-L.; Ogino, M.; Jiang, P. *Cryst. Growth Des.* **2009**, *9*, 4700−4705.
(65) Cobley, C.; Rycenga, M.; Zhou, F.; Li, Z.-Y.; Xia, Y. *Angew. Chem., Int. Ed.* **2009**, *48*, 4824−4827.
(66) Mahmoud, M. A.; Tabor, C. E.; El-Sayed, M. A. *J. Phys. Chem. C* **2009**, *113*, 5493−5501.
(67) Moran, C. H.; Rycenga, M.; Zhang, Q.; Xia, Y. *J. Phys. Chem. C* **2011**, *115*, 21852−21857.
(68) Cho, S. H; Han, H. S.; Jang, D. J.; Kim, K.; Kim, M. S. *J. Phys. Chem.* **1995**, *99*, 10594−10599.
(69) Joralemon, M. J.; O'Reilly, R. K.; Hawker, C. J.; Wooley, K. L. *J. Am. Chem. Soc.* **2005**, *127*, 16892−16899.
(70) Kim, S.; Bawendi, M. G. *J. Am. Chem. Soc.* **2003**, *125*, 14652−14653.
(71) Zeng, J.; Tao, J.; Li, W.; Grant, J.; Wang, P.; Zhu, Y.; Xia, Y. *Chem. Asian J.* **2011**, *6*, 376−379.
(72) Zhou, F.; Li, Z. Y.; Liu, Y.; Xia, Y. *J. Phys. Chem. C* **2008**, *112*, 20233−20240.